Arabian Journal for Science and Engineering
https://doi.org/10.1007/s13369-022-07401-4

RESEARCH ARTICLE-ELECTRICAL ENGINEERING

Faults Diagnosis of Rolling-Element Bearings Based on Fourier Decomposition Method and Teager Energy Operator

Mohamed Rebiai[1] · Mohamed Ould Zmirli[1] · Billel Bengherbia[1] · Sid Ahmed Lachenani[1]

Received: 20 November 2021 / Accepted: 16 October 2022
© King Fahd University of Petroleum & Minerals 2022

Abstract
Bearing failure is a common cause of machinery breakdown, resulting in lost production and accidents. Therefore, the early and automatic diagnosis of bearing faults is attracting increasing amounts of attention, in particular through vibration analysis. The vibration signals caused by rotating machines are multi-component and modulated signals; it is essential to demodulate after the components decomposition. Through the previous challenges, we have proposed an approach combining the most effective decomposition and demodulation techniques, namely the Fourier decomposition method (FDM) and the Teager energy operator (TEO). Next, we verified the FDM–TEO method's efficacy by applying it to synthetic and real bearing vibration signals and comparing it to other well-known methods using the FCFR assessment indicator. Comparative results were quite close, with the FDM–TEO and the empirical mode decomposition both having marginally better mean FCFRs than the variational mode decomposition method.

Keywords Vibration analysis · Feature extraction · Bearing diagnosis · Fourier decomposition · Teager energy operator

1 Introduction

Control and diagnosis are currently vital in most manufacturing processes. The monitoring of mechanical equipment is not complete without fault diagnostics utilizing a vibration signal. For this reason, many crucial industrial systems measure and evaluate vibration in real time alongside other parameters like temperature and acoustic measurements [1]. Rotating machines are present in industrial applications across the board. Additionally, bearings are crucial for sustaining loads and preserving clearances between rotating and stationary equipment, eliminating vibration and reducing the noise of rotating machines. But bearings are also one of the most common causes of mechanical failure. For instance, a statistical study has revealed that bearings cause a significant portion of motor failures [2]. In addition, another statistical analysis has found that faults with the bearing's inner and outer rings account for roughly 90% of bearing failures [3].

Different signal processing methods, including time-domain, frequency-domain, and time–frequency domain, can be used to analyse vibration signals to detect bearing faults. The temporal representation of the vibratory signal is not clear; therefore, extracting useful information is not enough to locate the fault; it can only predict its presence. In contrast, frequency techniques can determine the presence and location of bearing faults, such as the fast Fourier transform (FFT), the application of which to a vibration signal with a fault yields frequency peaks associated with the fault. Therefore, the location of the fault is possible. Despite the above, analysing non-stationary physical signals such as vibrations by frequency techniques is inefficient, but the time–frequency technique fixes the issue [4, 5].The wavelet theory is a basic time–frequency method, but it is unsuitable for nonlinear signals.

Through the shortcomings of the previous methods, we introduced modern decomposition methods, which remove all the previous inconveniences; that is, they are effective for nonlinear, non-stationary and multi-component signals The most important of these methods are EMD, VMD, and FDM. We chose the FDM method for use in the proposed approach because it is better than the other two methods. The first advantage of FDM comes from the fact that it has a solid mathematical basis, unlike EMD [6], which is empirical. Secondly, FDM does not require preset parameters, unlike VMD [7].

✉ Mohamed Rebiai
rebiaimd@gmail.com

[1] Research Laboratory in Advanced Electronics Systems LSEA, University of Médéa, Pole Urbain, 26000 Medea, Algeria

Published online: 15 November 2022

This article proposes a combined approach for fault diagnosis and feature extraction. First, FDM is used to decompose the vibration signal, then TEO is applied to all components to extract the envelope, and finally, the component that contains the most defect information is selected using $FCFR$, called the effective component, omitting the remaining components. The FCFR of the effective component can be used as a diagnosis parameter. The choice of the formula, FDM − FCFR-TEO, was never random but followed a theoretical analysis of each technique. The proposed method was validated using simulated and experimental data from normal and faulty bearings in the case Western Reserve university's ($CWRU$) database [8]. A comparative study with other well-known methods is presented. The rest of this paper has four main parts: a signal processing methods section, a process of the proposed method FDM - TEO section, and finally, the applications and results section. In the end, the conclusion is given.

2 Signal Processing Methods

2.1 Analytic Signal and Hilbert Transform

The analytical signal often used in signal processing is defined by a complex function without a negative frequency component, as follows: $x_a(t) = x(t) + j\widehat{x}(t)$, so $\widehat{x}(t) = \mathcal{H}\{x(t)\} = x(t) * (1/\pi t)$ is the Hilbert transform of $x(t)$, where $*$ is the convolution operation; and j is the imaginary unit. An expression in polar coordinates of the analytical signal can also be given by

$$x_a(t) = a(t)e^{j\phi(t)} \tag{1}$$

This polar representation introduces the following three quantities: the instantaneous amplitude (envelope)$a(t) = |x_a(t)|$, the instantaneous phase $\phi(t) = arg\{x_a(t)\}$, and the instantaneous frequency $f(t) = (1/2\pi)\cdot(d\phi(t)/\mathrm{d}t)$ in [Hz]. These instant quantities are used in many applications to measure and extract the local characteristics of the signal [9].

2.2 Fourier Decomposition Method

FDM Is a new signal processing method proposed by Singh et al. [4]. It is considered a time–frequency analysis tool, but it does not require any previously known basis, and is adaptive, unlike other time–frequency methods. Using FDM, any real and time-limited signal $x(t) \in [a, b]$ (multi-component, nonlinear, and nonstationary) can be decomposed into a sum of single-component, band-limited orthogonal signals $y_i(t) \in \mathbb{C}^{\infty}[a, b]$, named Fourier intrinsic band functions ($FIBF$) [4], as follows:

$$x(t) = \sum_{i}^{M} y_i(t) + a_0 \tag{2}$$

where M is the number of$FIBF$, a_0 is the average value of$x(t)$. The functions $y_i(t) = \{y_1(t), y_2(t), \ldots, y_M(t)\}$ satisfy the following three conditions: zero mean, orthogonal and the $FIBF$ admits an analytical representation ($AFIBF$). The mathematical expressions of these conditions are, respectively, given by:$\forall i$, $\int_a^b y_i(t)\mathrm{d}t = 0$; $\forall i \neq j$, $\int_a^b y_i(t)y_j(t)\mathrm{d}t = 0$;$y_i(t)+j\widehat{y}_i(t) = a_i(t)e^{j\phi_i(t)}$, where $\widehat{y}_i(t)$ the Hilbert transform of$y_i(t)$, $a_i(t) \geq 0$ is the instantaneous amplitude, and $\omega_i(t) = (d\phi_i(t)/dt) \geq 0$ is the instantaneous frequency.

We will now present how to decompose a discrete signal $x[n]$ of length N into a set of $FIBF$, so $X[k] = (1/N)\sum_{n=0}^{N-1} x[n]e^{-\frac{j2\pi kn}{N}}$ its discrete Fourier transform, we can express this signal as follows

$$x[n] = \sum_{k=0}^{N-1} X[k]e^{\frac{j2\pi kn}{N}} \tag{3}$$

Then, we can express $x[n]$ as follows:

$$\begin{aligned} x\,[n] = X\,[0] + &\sum_{k=1}^{\frac{N}{2}-1} X[k]e^{\frac{j2\pi kn}{N}} \\ &+ X\,[N/2]\,e^{j\pi n} + \sum_{k=\frac{N}{2}+1}^{N-1} X[k]e^{\frac{j2\pi kn}{N}} \end{aligned} \tag{4}$$

Since $x[n]$ and the first and third terms on the right side of Eq. (4) are real, this equation's second and fourth terms are complex conjugates. Equation (4) can be simplified as follows:

$$x[n] = X[0] + 2Re\{z[n]\} + (-1)^n X[N/2] \tag{5}$$

where $Re\{\cdot\}$ denote the real part and $z[n] = \sum_{k=1}^{\frac{N}{2}-1} X[k]e^{\frac{j2\pi kn}{N}}$ is an analytical signal, we write it as follows:

$$z[n] = \sum_{i=1}^{M} a_i[n]e^{j\phi_i[n]}. \tag{6}$$

AFIBFs can be obtained from the signal in backward search order (i.e. frequency scan from high to low), the first AFIBF is $a_1[n]e^{j\phi_1[n]} = \sum_{k=N_1}^{N_0-1} X[k]e^{\frac{j2\pi kn}{N}}$, the second AFIBF is $a_2[n]e^{j\phi_2[n]} = \sum_{k=N_2}^{N_1-1} X[k]e^{\frac{j2\pi kn}{N}}$,..., the ith

AFIBF is

$$a_i[n]e^{j\phi_i[n]} = \sum_{k=N_i}^{N_{i-1}-1} X[k]e^{\frac{j2\pi kn}{N}} \tag{7}$$

With $N_0 = N/2, N_i = 1$. For each i, N_i is scanned from $N_{i-1} - 1$ to 1 and keeping the minimum value that meets the following conditions: the instantaneous amplitude $a_i[n] \geq 0$ and the instantaneous frequency $f[n] = (\phi_i[n+1] - \phi_i[n])/2\pi$ in $N_i \in [1, N_{i-1} - 1]$. For additional information on the FDM Algorithm, we refer to [4]. A MATLAB code of FDM is available online at [10].

2.3 Teager Energy Operator *TEO*

In the last thirty years, many researchers have introduced and investigated an impressive nonlinear operator named Teager Energy Operator (or Teager–Kaiser Energy Operator) in diverse applications, particularly in the AM-FM signal processing, such as the signal of speech [11].The attractiveness of this operator is due to its small time window (ideal for analysing signals locally), and the simplicity of its basic definition [12]. This operator can demodulate an AM-FM signal and extract the instantaneous amplitude (the envelope signal) and instantaneous frequency of a mono-component signal.

In the proposed method, the TEO is applied to the $FIBF$ obtained by the Fourier decomposition method for envelope demodulation of mono-component $FIBF$, which increases the characteristic faults, thus facilitating its extraction [13].

For $y(t)$ a continuous-time signal, $\dot{y}(t)$ its first derivative and $\ddot{y}(t)$ its second derivative. The simplified form of TEO of continuous-time t is defined as Eq. (8):

$$\Psi\{y(t)\} = \dot{y}^2(t) - y(t) \cdot \ddot{y}(t) \tag{8}$$

For obtaining the TEO of a discrete-time signal $x[n]$, the TEO can be redefined by simply changing the derivative with the difference in Eq. (8). We get the following equation:

$$\Psi\{y[n]\} = y^2[n] - y[n-1] \cdot y[n+1] \tag{9}$$

where n is the number of samples. More details about TEO can be found in [12] and [11].

2.4 Fault Characteristic Frequency Ratio "FCFR"

In this work, we need an indicator to assess the fault information. However, many indicators are commonly used in many applications, for example, kurtosis, Shannon entropy principle, and correlation coefficient [14]. But, the component selected by these indicators cannot automatically contain most fault frequency information [15]. For this reason, the FCFR value is introduced in this paper to select the FIBF which contains the largest fault frequency component by calculating the proportion of fault characteristic frequency f_c and its harmonics in the envelope spectrum. FCFR can be expressed as follows:

$$\text{FCFR} = \left(\sum_{i=1}^{n} |E(i \cdot f_c)|\right) \Big/ \left((1/N)\sum_{i=1}^{N} |E(i \cdot f)|\right) \tag{10}$$

where E is the envelope spectrum of $FIBF$ obtained by TEO, f is the frequency resolution and N is the number of points in the envelope spectrum, $i \cdot f_c$ and $i \cdot f$ are the ith harmonic of f_c and f, respectively.

We can calculate the FCFR_i and FCFR_o of the inner ring fault and outer ring fault, respectively, substituting the fault characteristic frequency f_c by the inner ring fault frequency f_i and the outer ring fault frequency f_o in Eq. (10), respectively.

A basic envelope spectrum analysis reveals that most fault information is contained in the first three harmonics. Consequently, just the range of the three envelope spectra is taken into account by substituting $n = 3$ and $N = 3f_c$ into Eq. (10), which also reduces the influence of noise [14].

3 Process of the Proposed Method *FDM-TEO*

Figure 1 shows a flow diagram of the detailed calculation procedure of the proposed method, based on the DM and TEO. The following steps explain the procedure:

- The FDM is used to decompose a bearing vibration signal into n mono-component signals called "$FIBF$".
- Calculating the TEO of each component FIBF according to Eq. (9), then application of the FFT operator to obtain the envelope spectrum.
- Determining the FCFR of the envelope spectrum according to Eq. (10), the FIBF with the largest FCFR is chosen as the effective component, and its envelope spectrum is analysed for bearing faults detection.
- The largest FCFR_i and FCFR_o are compared to a predetermined threshold δ_d to determine the presence of faults as well as their types.

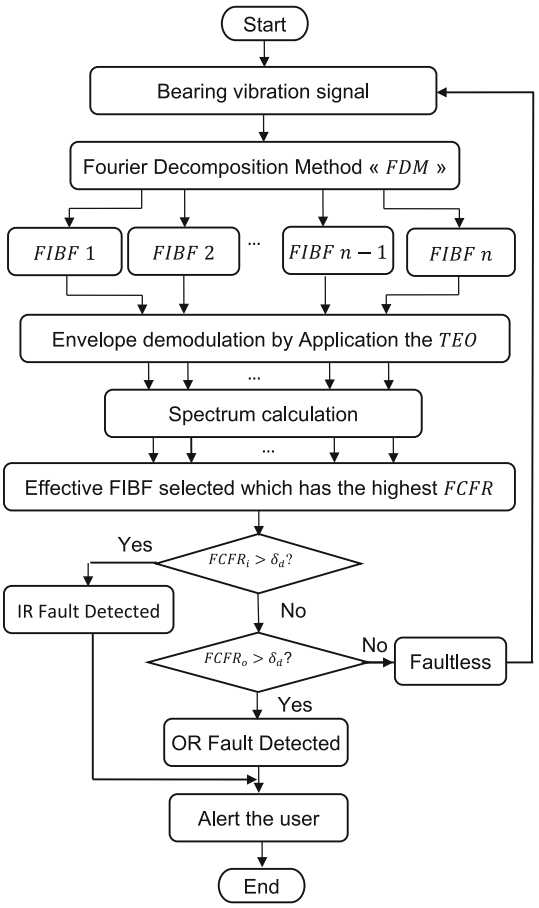


Fig. 1 Flow chart of Bearing fault diagnosis based on FDM-TEO

4 Applications and Results

4.1 Capability of Separation

We used the technique for evaluating the performance of EMD provided in [16] and [17] to evaluate the decomposition capability of FDM. For this purpose, the following signal $x_{\mathrm{sig1}}(t)$ is used, which consists of two pure harmonics f_1 and f_2 of amplitudes a_1 and a_2, respectively, sampled at 1 [Hz].

Table 1 Parameters of the simulation signals

Symbol of synthetic signals		sim_{IR}	sim_{OR}
Parameters of synthetic signal $x(t)$	A	0.01	0.01
	f_r[Hz]	10	10
	f_n[Hz]	2500	4000
	f_s[Hz]	12,000	12,000
	α	90	900
	B	$0.15\sin(2\pi f_r t)$	0.25
	f_c[Hz]	$f_i = 150$	$f_o = 100$
	$n(t)$[dB]	− 10	− 10

$$x_{\mathrm{sig1}}(t) = a_1\cos(2\pi f_1 f_s t) + a_2\cos(2\pi f_2 f_s t) \tag{11}$$

The relative error e_r of the extraction can be quantified by Eq. (12). Where $x_{hf}(t)$ is the high-frequency harmonics in $x_{sig1}(t)$ and $Ex_{hf}(t)$ represents the high-frequency component obtained after decomposition by FDM, and $\|\cdot\|_2$ represents the l_2 norm of a vector. This equation is the indicator for evaluating the extracted high-frequency harmonic, which used to measure the separation capacitance.

$$e_r = min\left(\|x_{hf}(t) - Ex_{hf}(t)\|_2 / \|x_{hf}(t)\|_2,\ 1\right) \tag{12}$$

$e_r = 0$ indicates the entirely extraction of high-frequency harmonic $Ex_{hf}(t)$ from $x_{sig1}(t)$. But, $0 < e_r \leq 1$ indicates that the separation between two harmonics is not completely.

Figure 2 illustrates the relative error e_r with values between 0 (black) and 1 (white) at different amplitudes (a_1, a_2), the blackest pixels correspond to smaller errors. In

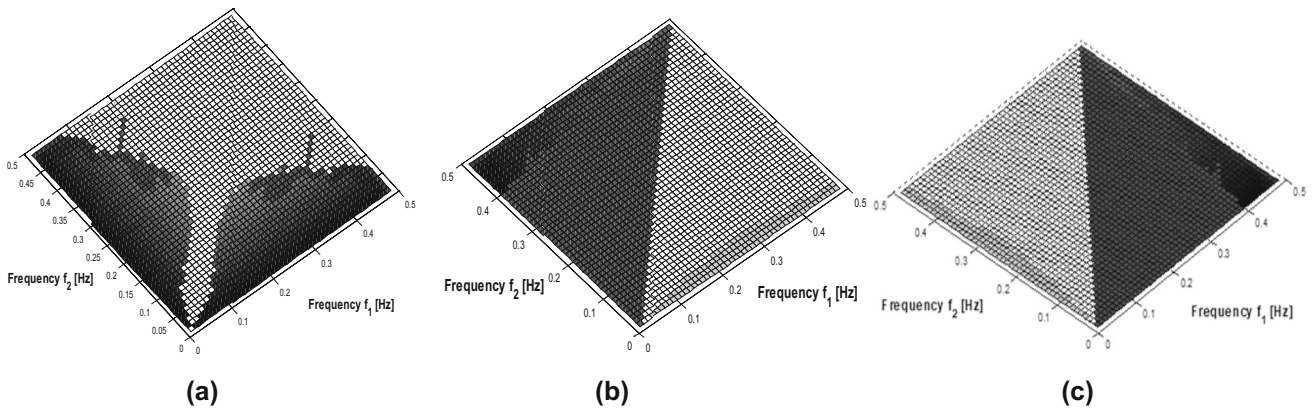


Fig. 2 Decomposition ability of FDM: **a** with $a_1 = a_2 = 4$, and $0 \leq f_1 \leq 0.5$, $0 \leq f_2 \leq 0.5$ (**b**) with $a_1 = 1$, $a_2 = 4$, $0 \leq f_1 \leq 0.5$, $0 \leq f_2 \leq 0.5$ and (**c**) with $a_1 = 4$, $a_2 = 1$ $0 \leq f_1 \leq 0.5$, $0 \leq f_2 \leq 0.5$

other words, black pixels correspond to the complete separation of the high-frequency harmonic, while grey and white pixels correspond to partial separation and non-separation, respectively. We can easily deduce from this the difficulty of separation in FDM for high-frequency harmonics when these frequencies are close to the sampling frequency.

4.2 Application on Simulated Signals

In this part, we validate the proposed method $TEO\text{-}FDM$ for the detection of bearing faults, according to the bearing fault model developed from three references ([14, 18], and [19]). Therefore, the proposed synthetic signal $x(t)$, which emulates the vibration of the bearing, with inner ring fault and outer ring fault, is generated as follows:

$$x(t) = A\cos(2\pi f_r t) + \sum_{k=0}^{\infty} Be^{-\alpha(t-kT_c)}\sin(2\pi f_n(t-kT_c)) + n(t) \quad (13)$$

where A and f_r are the amplitude of shaft vibration and the rotating frequency, respectively, B is the amplitude of vibration caused by a fault (outer ring or inner ring), and $f_c = 1/T_c$ represents fault frequency ($f_c = f_i$ for inner ring fault or $f_c = f_o$ for outer ring fault),α is the attenuation coefficient, f_n is the resonance frequency and $n(t)$ is the Gaussian white noise. The specific parameters of $x(t)$ to build the two simulation signals (inner faults and outer faults) are presented in Table 1.

The waveforms of the two simulated signals sim_{0R} and sim_{IR} without noise, sampled at12000[Hz], are shown in Figs. 3a and 4a, respectively. The noisy signals are shown in Figs. 3b and 4b, which are produced using the MATLAB function "$randn$" with an SNR $= -10$ dB. The FFTs of the two signals sim_{0R} and sim_{IR} are shown in Figs. 3c and 4c, respectively. We see on these two spectral figures that the frequencies of the faults (f_i, f_o) are invisible. Also, from the enlarged view of the frequency-domain waveform for the low-frequency region shown in Figs. 3d and 4d, the observation of fault frequencies is impossible, and the impact signals are entirely flooded by noise. Moreover, the proportion values of fault characteristic frequencies f_o and f_i in the spectra of sim_{or} and $\mathrm{sim_{ir}}$ are $\mathrm{FCFR}_o = 5.42$ and $\mathrm{FCFR}_i = 4.09$, respectively. Therefore, the dominant frequencies are not f_i and f_o, and it is not easy to extract the fault characteristics by time-domain and FFT analysis.

The FDM-TEO algorithm is applied to the synthetic signals to extract the characteristic frequencies of faults ($f_o = 100$[Hz] and $f_i = 150$[Hz]). We get fifty tow components for each signal, as shown in Figs. 5 and 6 for simulation signals sim_{IR} and sim_{OR}, respectively. Due to the large number of components obtained after decomposition and the limited space, we show only six components that contain the most effective $FIBF$.

The FCFR_i of all $FIBF$ of sim_{ir} are calculated by Eq. (10) and are listed in Table 2. The FIBF with the largest FCFR_i is considered the most effective $FIBF$. From Table 2, the FIBF26 is selected as the most effective component. Similarly, the FCFR_o of all FIBF of $\mathrm{sim_{or}}$ are also calculated by Eq. (10). The results are listed in Table 3. According to this table, FIBF22 is selected as the most effective component.

From the result shown in Fig. 7b, we can see the characteristic frequency of the simulated inner ring fault (150[Hz])

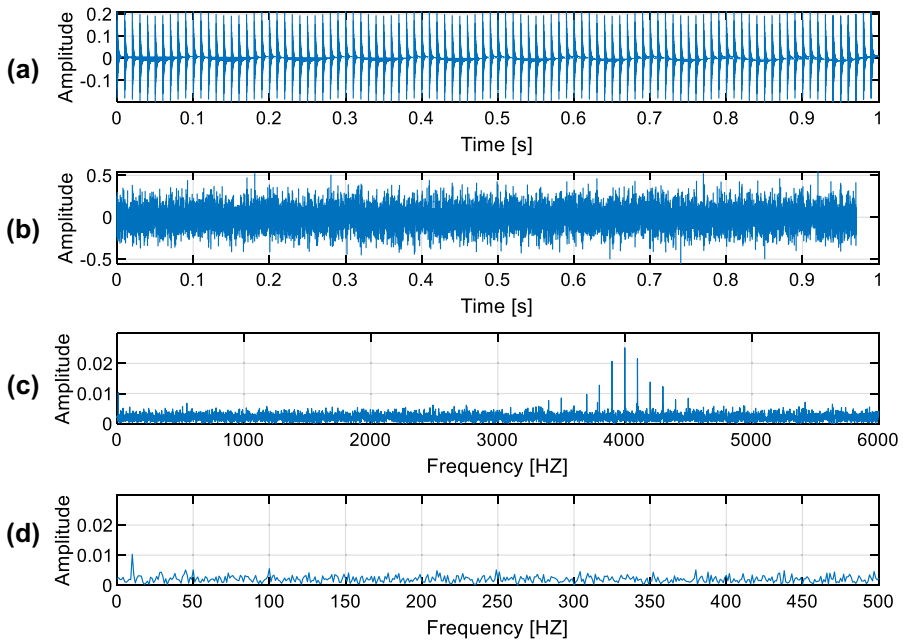


Fig. 3 Simulated outer ring faultsim_{0R}: **a** Time-domain waveform without noise; **b** Time-domain waveform with noise (SNR $= -10$ dB); **c** Frequency-domain waveform; **d** Enlarged view of the frequency-domain waveform

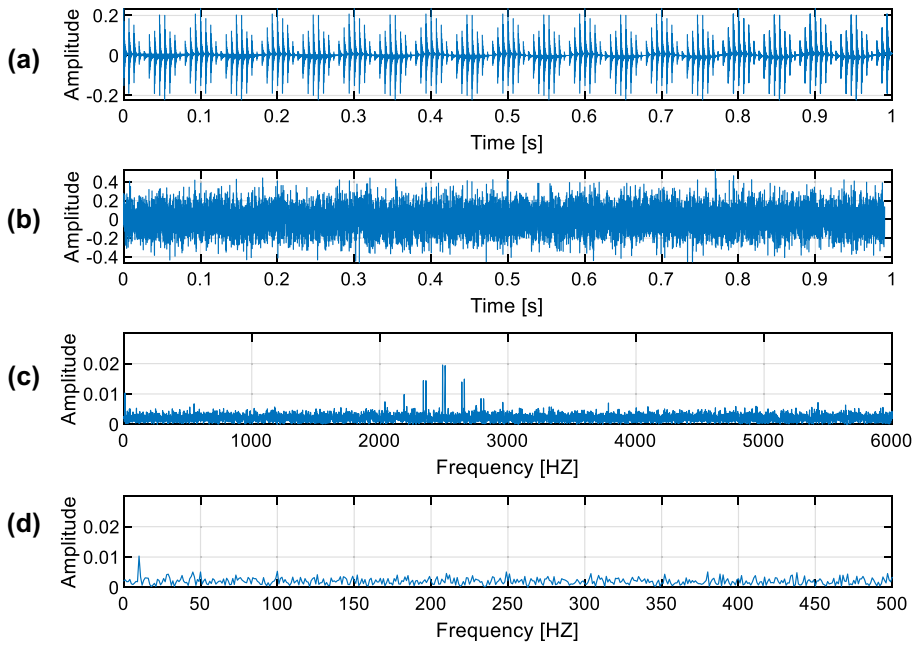


Fig. 4 Simulated inner ring faultsim_{IR}: **a** Time-domain waveform without noise; **b** Time-domain waveform with noise (SNR $= -10$ dB); **c** Frequency-domain waveform; **d** Enlarged view of the frequency-domain waveform

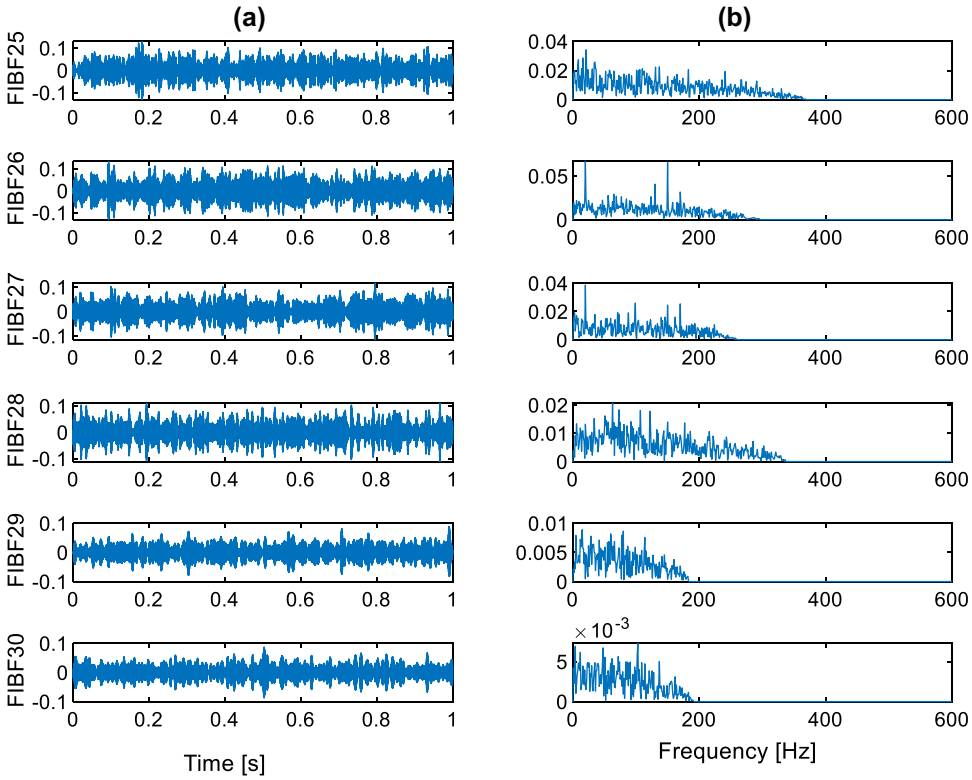


Fig. 5 Decomposition results of simulation signal sim_{IR} using $FDM\text{-}TEO$; **a** The time-domain waveform of some FIBF; **b** Envelope spectrum of these FIBF

demodulated from the amplitude spectrum FIBF26 and centred at the high-frequency resonance band (2500[Hz]) shown in Fig. 7a. Overall, the frequency of a rotation and the characteristic frequencies, as well as their harmonics that are clearly identified on the envelope spectrum, show that the fault characteristic is indeed extracted by the proposed method.

As shown in Fig. 8b, the twenty-second component includes the characteristic frequency of the simulated outer ring fault (100[Hz]), and its second-order harmonic (200[Hz]) demodulated from the amplitude spectrum $FIBF22$ centred at the high-frequency resonance band (4000[Hz]) as shown in Fig. 8a, which indicates that the fault extraction of the simulated outer ring fault is ideal.

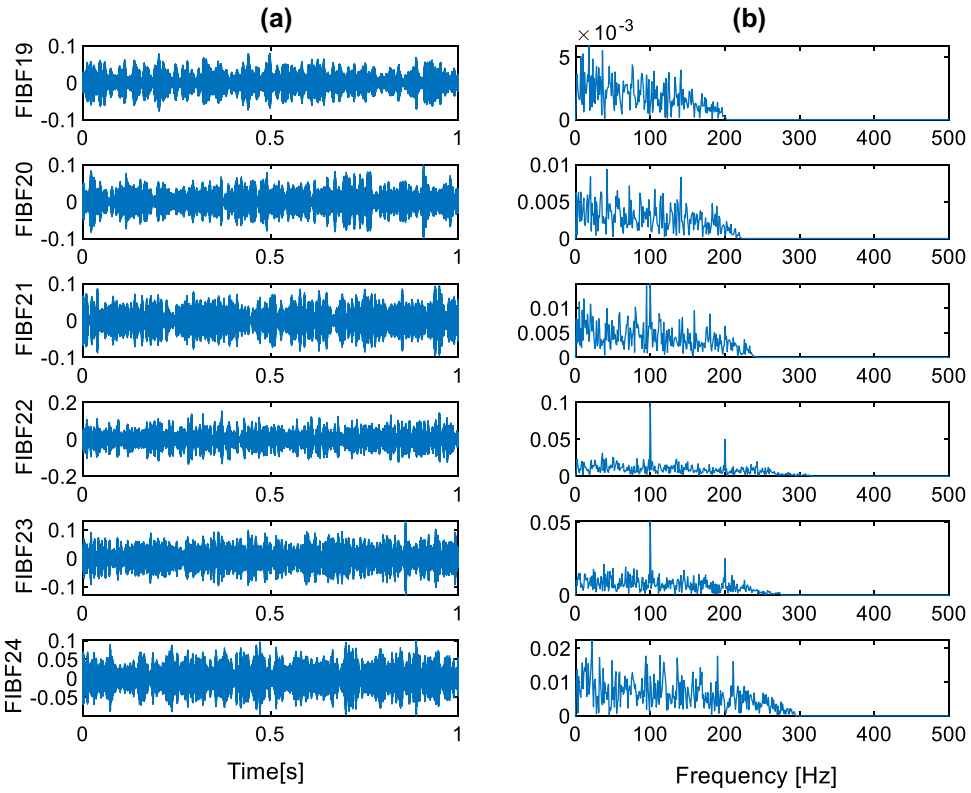


Fig. 6 Decomposition results of simulation signal sim_{OR} using FDM-TEO; **a** Time-domain waveform of some FIBF; **b** Envelope spectrum of these FIBF

Table 2 $FCFR_i$ of all FIBF obtained by FDM-TEO decomposition results of the simulation signal sim_{IR}

FIBF	$FCFR_i$	FIBF	$FCFR_i$	FIBF	$FCFR_i$	FIBF	$FCFR_i$
1	0.0000	14	0.0001	27	6.2087	40	0.0000
2	0.0000	15	0.0000	28	4.3996	41	0.0012
3	0.0000	16	0.0000	29	1.7292	42	0.0000
4	0.0000	17	0.0000	30	1.9279	43	0.0328
5	0.0000	18	0.0001	31	3.1994	44	0.0000
6	0.0000	19	2.4312	32	0.0001	45	0.0000
7	0.3806	20	2.7545	33	0.0000	46	0.0043
8	0.0000	21	2.1132	34	0.0001	47	0.0000
9	0.0724	22	3.3811	35	0.0000	48	0.0000
10	0.0000	23	1.5867	36	0.0001	49	0.0000
11	0.0000	24	1.3931	37	0.0000	50	0.0000
12	0.0000	25	3.0962	38	0.0000	51	0.0000
13	0.0001	***26***	***9.7786***	39	0.0001	52	0.0000

Bold italic values indicate the most effective component

4.3 Noise Impact on the Proposed Approach Performance

To confirm FDM-TEO efficacy in fault diagnostics in more detail. We investigate the impact of background noise (SNR between − 2 dB and − 20 dB) on the performance of the proposed approach. Table 4 and Fig. 9 demonstrate how decreasing the SNR results in a lower FCFR value. Therefore, early bearing fault identification from the vibration signal with SNR less than − 16 dB is impossible because the FCFR values are low.

4.4 Application on Measured Signals

After using synthetic data in the previous part, we now assess the proposed method on measured vibration signals issued from bearings in rotating machines.

Table 3 $FCFR_o$ of all $FIBF$ obtained by $FDM\text{-}TEO$ decomposition of the simulation signal sim_{OR}

FIBF	$FCFR_o$	FIBF	$FCFR_o$	FIBF	$FCFR_o$	FIBF	$FCFR_o$
1	0.0000	14	1.2861	27	3.1545	40	0.0000
2	0.0000	15	0.6052	28	3.9459	41	0.0000
3	0.0000	16	1.7126	29	3.0025	42	1.5351
4	0.0000	17	0.9980	30	2.8544	43	0.0000
5	0.0000	18	1.7305	31	1.4854	44	0.0000
6	0.1168	19	2.8169	32	4.0475	45	0.0032
7	0.0000	20	3.4980	33	1.5833	46	0.0000
8	0.0214	21	6.7000	34	1.1000	47	0.0109
9	0.0763	***22***	***16.1750***	35	1.5776	48	0.0000
10	0.0000	23	12.0753	36	2.9385	49	0.1651
11	0.0000	24	2.8223	37	0.0000	50	0.0000
12	0.0000	25	3.3630	38	1.0831	51	0.0000
13	0.0000	26	3.1003	39	0.0001	52	0.0000

Bold italic value indicates the most effective component

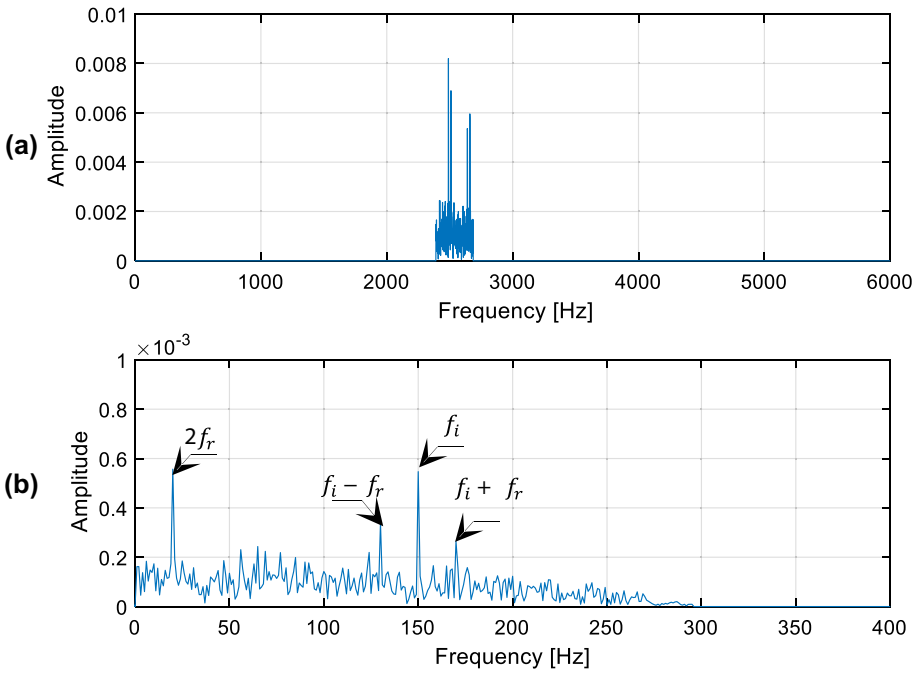


Fig. 7 Spectra of the twenty-sixth component "$FIBF26$" obtained by FDM-TEO of simulation signal sim_{IR}: **a** Amplitude spectrum; **b** Envelope spectrum

4.4.1 Description of the CWRU Dataset

This work exploits the experimental database of vibration signals from various faulty parts of the bearing, introduced by Case Western Reserve University as an open-source database [20].

A simplified schematic platform for the CWRU bearing test apparatus is shown in Fig. 10. The test data contain different situations of measurements of normal and faulted bearings under various conditions such as motor speed (1730, 1750, 1772 and 1797 [rpm]), motor load (0, 1, 2 and 3 [hp]), sample frequency (12 or 48 [kHz]), bearing details (Drive end bearing DE: 6205-2RS *JEM SKF*, or fan end bearing FE: *6203-2RS JEM SKF*) and fault diameter (0.1778, 0.3556 and 0.5334 [mm]).

The vibration signal obtained from the vibration sensor (generally a piezoelectric accelerometer) is a multi-component signal. Each part of the bearing participates with a frequency component. The bearing contains four pieces: an outer ring, an inner ring, a ball and a cage (Fig. 11a). Each component of this bearing can be affected by a local fault (Fig. 11b) when the ball passes over the local fault, so a fault frequency is obtained for each part: cage frequency, ball spinning frequency, outer ring frequency, inner ring frequency, and rolling-element (ball) frequency. Therefore, the defects increase the vibrational energy at different

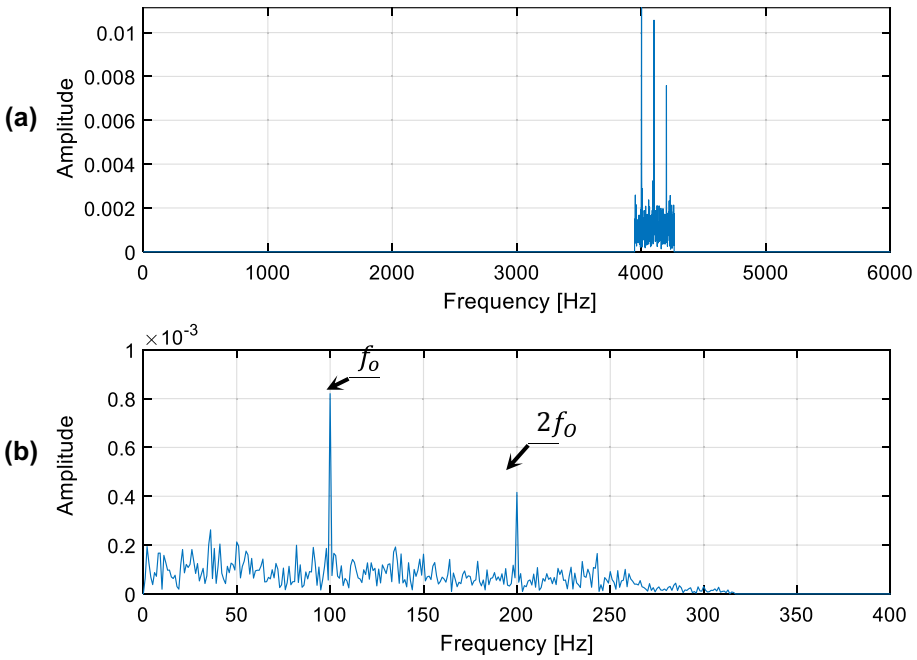


Fig. 8 Spectra of the Twenty-tow component "FIBF22" obtained by FDM-TEO of simulation signal sim_{OR}; **a** Amplitude spectrum; **b** Envelope spectrum

Table 4 Variation of FCFR of sim_{IR} and sim_{OR}, as a function of noise

FCFR of	Signal-to-noise ratio (SNR)									
	− 2 dB	− 4 dB	− 6 dB	− 8db	− 10 dB	− 12 dB	− 14 dB	− 16 dB	− 18 dB	− 20 dB
sim_{IR} obtained by proposed approach	26.58	24.01	20.27	9.29	9.78	7.69	6.59	4.59	5.07	4.57
sim_{OR} obtained by proposed approach	33.93	24.33	24.99	24.04	16.15	13.70	12.75	7.29	7.13	7.00

frequencies of the bearing components. Below are the characteristic frequencies for each piece [8, 21].

The ball-pass frequency at the inner ring (BPFI):

$$f_i = (N/2) \cdot F \cdot (1 + (B/P)\cos\alpha)[\text{Hz}] \tag{14}$$

The ball-pass frequency at the outer ring (BPFO):

$$f_o = (N/2) \cdot F \cdot (1 - (B/P) \cdot \cos\alpha)[\text{Hz}] \tag{15}$$

The ball-spin frequency (BSF):

$$f_b = (P/B) \cdot (F/2) \cdot \left(1 - ((B/P) \cdot \cos\alpha)^2\right)[\text{Hz}] \tag{16}$$

The fundamental train frequency (FTF):

$$f = (F/2) \cdot (1 - (B/P) \cdot \cos)[\text{Hz}] \tag{17}$$

Equations (14) to (17) are the characteristic frequency formulas for a fixed outer ring bearing, where $F = n/60$ is the shaft rotation frequency in$[Hz]$, n is the motor speed in [rpm], N is the number of rolling elements, and α represents the contact angle of the balls in [rad]. B and P are, respectively, the ball diameter's and pitch circle's diameter in[mm]. Figure 12 shows the effect of these fundamental frequencies on the bearing vibration signal [22]. Also, changes in the speed and load of a rotating machine lead to changes in vibration.

This study is restricted to diagnosing only the faults of the most common (inner and outer rings) compared with normal bearing (faultless). As a result, we chose twelve specific cases from this large amount of data, as mentioned in Table 5.

Table 5 provides information on the vibration signals used in this study, collected from three different bearings (inner ring fault, outer ring fault and faultless) for different motor speeds and loads, where the diameter of the fault is 0.18 [mm]. All vibration signals are sampled at a rate of 12 [kHz], and the fundamental frequencies f_i, f_o, f_b and f are calculated by Eq. (14) to Eq. (17), respectively. A one-second slice of each vibration signal described in Table 5 is shown in Fig. 13.

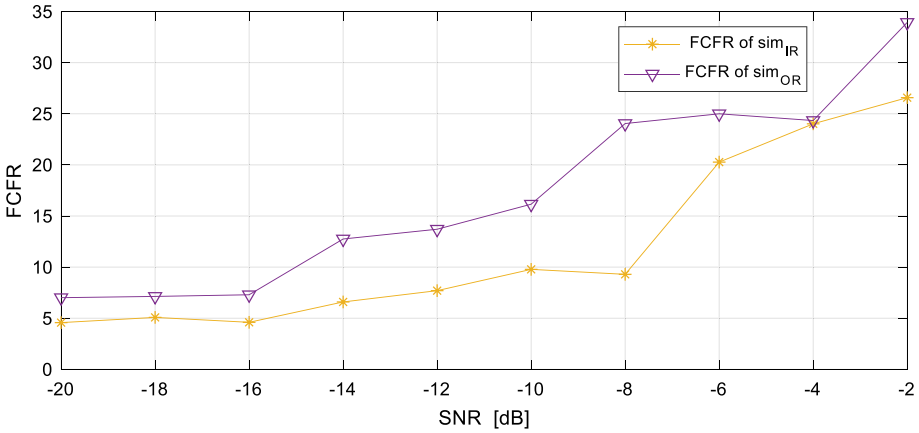


Fig. 9 The noise impact on the proposed method performance

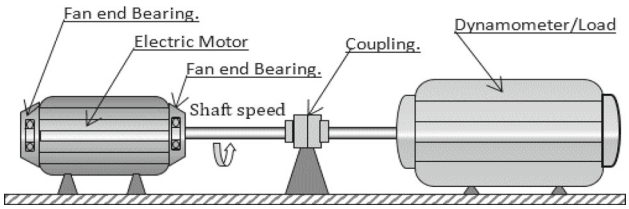


Fig. 10 Diagram of bearing fault test bench

The representation in the frequency domain of these vibration signals obtained by applying of the fast Fourier transform is presented in Fig. 14.

As shown in Fig. 14, the spectra of the faulty bearings indicate an increase in energy and large peaks in the high-frequency range (between 2 and 4 kHz). Therefore, the characteristic fault frequencies, f_i, f_o less than 200 Hz, are not dominant or prominent in these spectra, which will be explained in detail, with specific examples in subsections B and C below. This increase in energy designates the existence of a fault (due to the characteristic frequencies and the additional harmonics resulting from combinations between them). However, there is no sufficient information about the failed part of the bearing due to the weakness of the fault frequency peak, making it indistinguishable, as already confirmed in [23].

4.4.2 Bearing with Inner Ring Fault sig_{IR0}

To begin with, the waveforms of the first vibration signal of a bearing with an inner ring fault sig_{IR0} sampled at12[kHz], its FFT spectrum and the zoomed low-frequency spectrum are presented in Fig. 15. From Fig. 15, we can notice that the first three amplitudes of $BPFI$ (f_i,$2f_i$,$3f_i$, where $f_i = 162$[Hz]) are not prominent in the enlarged view for the low-frequency region ofsig_{IR0}, and some other frequencies in the neighbourhood of $BPFI$ have comparatively larger amplitudes.

Therefore, this signal was decomposed by FDM − TEO to separate the component containing the most significant characteristic frequency of the fault (i.e. the $FIBF$ with larger FCFR$_i$) from the original signal sig_{IR0}. Figure 16 displays the analysis result of the FDM-TEO method. With FDM decomposition, eighty-five FIBFs are obtained from

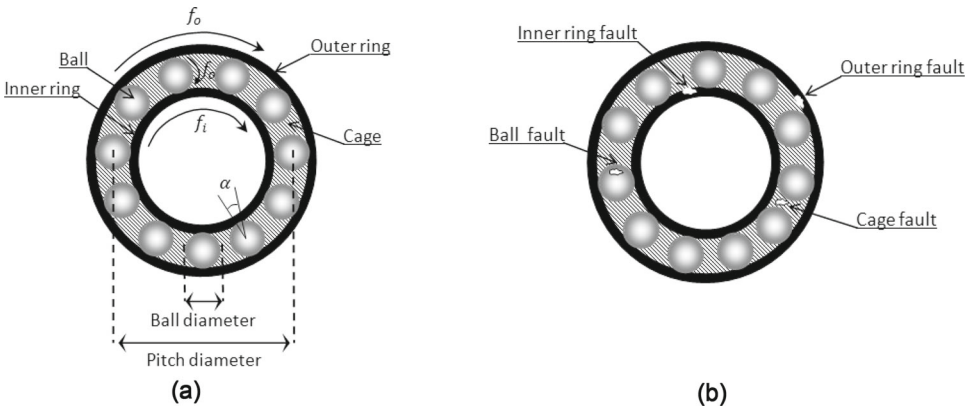


Fig. 11 A simple schematic of a ball bearing, **a** parts of ball bearing, **b** possible defects in a bearing

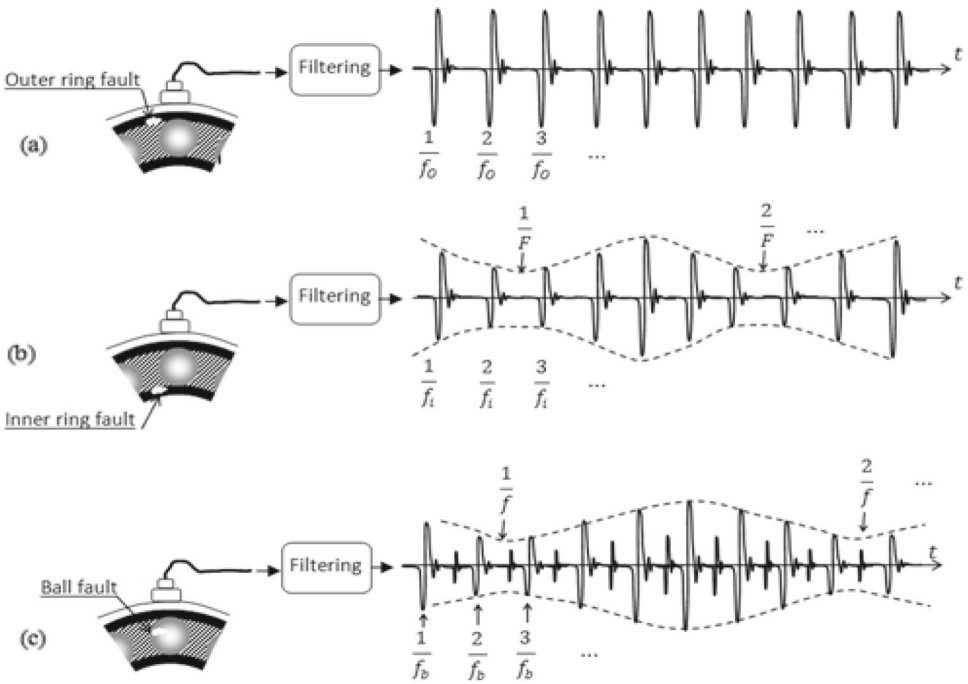


Fig. 12 Time-domain waveforms of vibration signals of bearing, **a** outer ring fault, **b** inner ring fault, **c** ball fault

Table 5 Parameters of bearing vibration signals used in this study

Bearing Details	Motor details		Sample rate [KHz]	Bearing fundamental frequencies [Hz]					Fault details		Symbol of vibration signal data in this study
	Motor speed n [rpm]	Motor Load [HP]		Shaft frequency F	$BPFI$ f_i	$BPFO$ f_o	BSF f_b	FTF f	Fault Diameter [mm]	Place of fault	
6205-2RS JEM SKF = 0;N=9;B = 7.94[mm]; P = 39.04[mm]	1797	0	12	29.95	162.19	107.36	141.17	11.93	0.18	Inner ring	sig_{IR0}
										Outer ring	sig_{0R0}
										Faultless	sig_{FL0}
	1772	1	12	29.53	159.93	105.87	139.20	11.76	0.18	Inner ring	sig_{IR1}
										Outer ring	sig_{0R1}
										Faultless	sig_{FL1}
	1750	2	12	2917	157.94	104.53	137.48	11.62	0.18	Inner ring	sig_{IR2}
										Outer ring	sig_{0R2}
										Faultless	sig_{FL2}
	1730	3	12	28.83	156.14	103.36	135.91	11.48	0.18	Inner ring	sig_{IR3}
										Outer ring	sig_{0R3}
										Faultless	sig_{FL3}

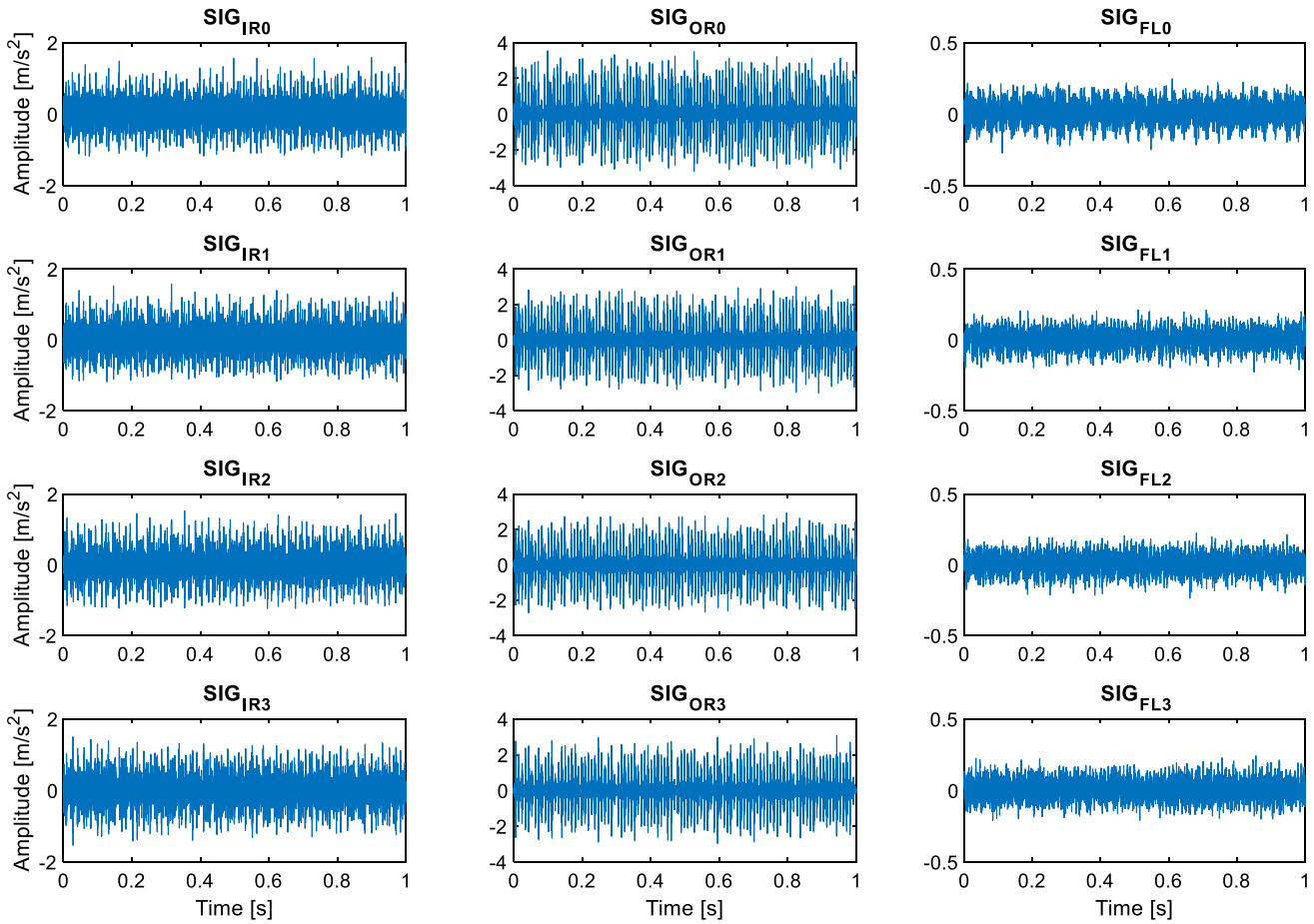


Fig. 13 A one-second slice of each vibration signal described in Table 5

the vibration signal sig_{IR0}. Then, the Teager Energy Operator TEO is used to demodulate each $FIBF$ component to obtain its envelope signal. Due to the limited space, only six components that contain the most effective FIBF(in this case, the most effective is the sixty-fifth component FIBF65) are shown in Fig. 16a, and their envelope spectra are shown in Fig. 16b.

The time-domain waveform, amplitude and envelope spectrum of the most effective component $FIBF65$ are presented in Fig. 17. From the result shown in Fig. 17c, we can see the characteristic frequency of the sig_{IR0} ($f_i = 162$[Hz]) demodulated from the amplitude spectrum $FIBF65$ and centred on the high-frequency resonance band (1.2to1.5[kHz]) shown in Fig. 17b. The proportion values of characteristic frequencies f_i and f_o in the spectrum of sig_{IR0} are given by $FCFR_i = 24.58$ and $FCFR_o = 7.27$, respectively. Overall, the rotational frequency and the characteristic frequencies, as well as their harmonics, are clearly identified on the envelope spectrum. On the other hand, the outer ring fault frequency f_o and its harmonics are undetectable. Therefore, we can easily deduce that the bearing from which this signal originates contains an inner ring fault and that there is no outer ring fault. Consequently, the fault characteristic is indeed extracted by the proposed method.

4.4.3 Bearing with Outer Ring Fault

This time, $FDM-TEO$ is used to analyse the vibration signal with outer ring fault sig_{OR0} to obtain its characteristic fault frequency ($f_O = 108$[Hz]). The waveform of the vibration signal sig_{OR0}, its FFT spectrum and the zoomed low-frequency spectrum are presented in Fig. 18. As shown in Fig. 18c, the first three $BPFO$ (f_o,$2f_o$, $3f_o$) amplitudes are not prominent, and several other frequencies in the f_o neighbourhood have relatively higher amplitudes. Therefore, the characteristic fault frequencies are not evident in the enlarged view for the low-frequency region of the sig_{OR0}. In this context, and through the proposed approach, we can make these characteristic frequencies prominent and easy to detect. Therefore, this signal was decomposed by FDM-TEO to separate the component containing the most significant characteristic frequency of the fault (i.e. the $FIBF$ with larger $FCFR_o$) from the original signal sig_{OR0}. Figure 19 shows

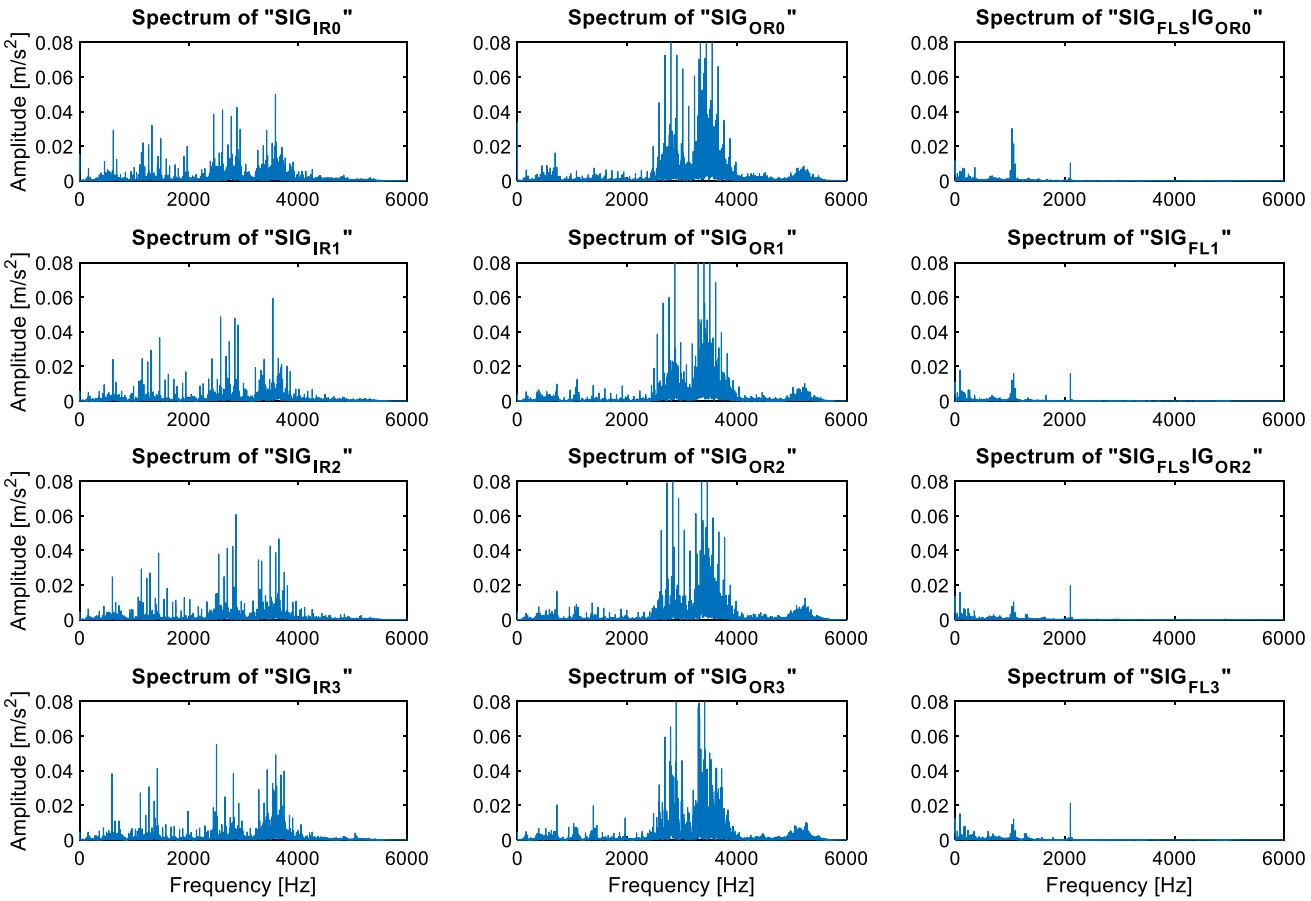


Fig. 14 Spectra of vibration signals listed in Table 5, obtained by application of the FFT operator

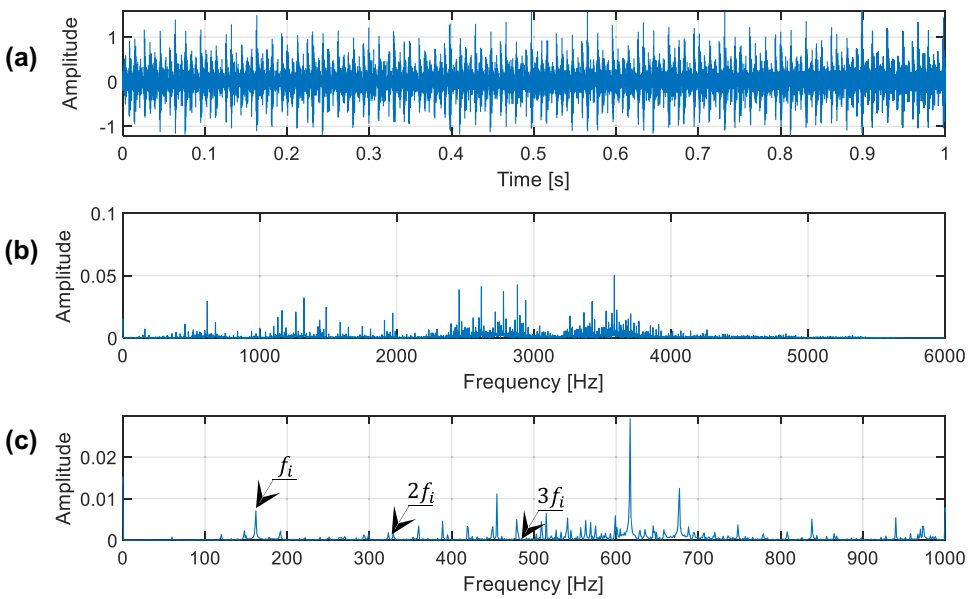


Fig. 15 Measured vibration signal sig_{IR0}: **a** Time-domain waveform; **b** Frequency-domain waveform; **c** Enlarged view of the frequency-domain waveform ($f_i = 162.19$[Hz])

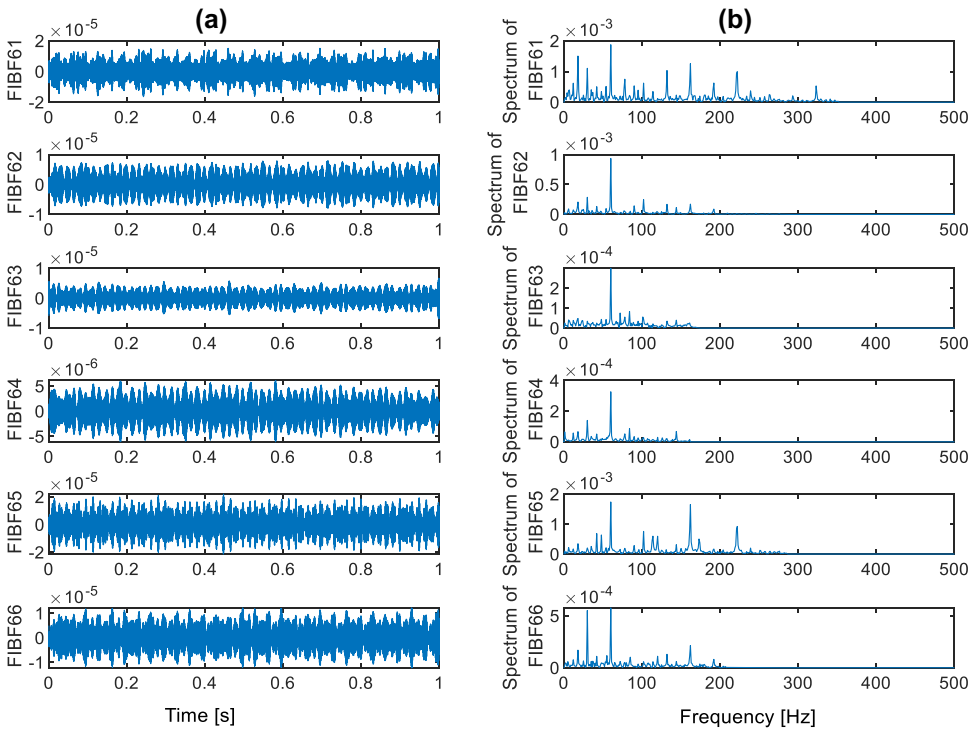


Fig. 16 Decomposition results of the measured signal sig_{IR0} using FDM-TEO; **a** Time-domain waveform of some components FIBF; **b** Envelope spectrum of these FIBF

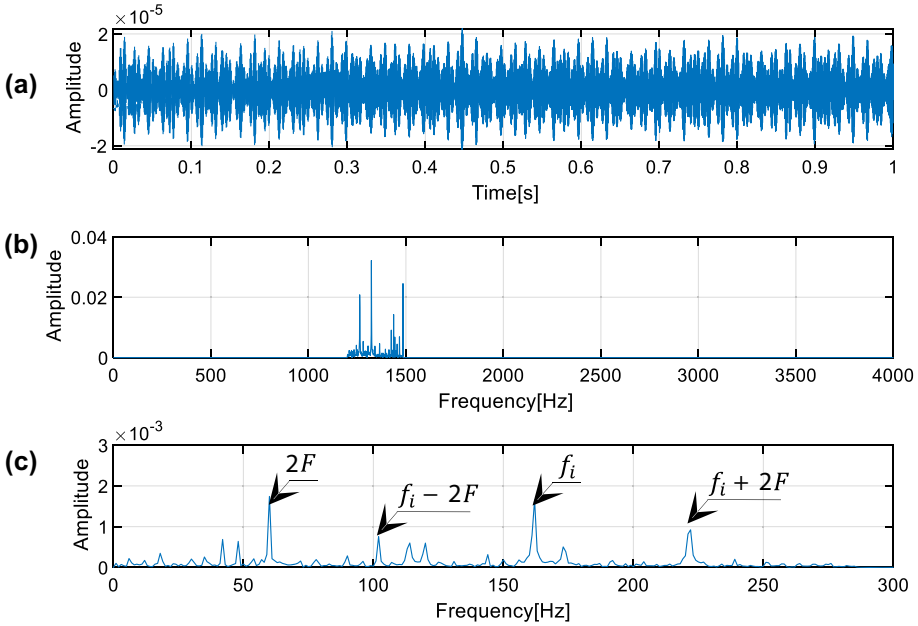


Fig. 17 Spectra of the sixty-fifth component $FIBF65$ obtained by FDM-TEO of signal sig_{IR0}: **a** Time-domain waveform; **b** Frequency-domain waveform; **c** Envelope spectrum ($f_i = 162.19$[Hz] fault frequency, $F = 29.95$[Hz] shaft frequency)

the analysis result of the $FDM\text{-}TEO$ method, and twenty-four $FIBFs$ are obtained from the vibration signal sig_{OR0}. But, only the first six components which contain the most effective $FIBF$ (in this case, the most effective is the first component $FIBF1$) are shown in Fig. 19a, and their envelope spectra are shown in Fig. 19b.

Figure 20 shows the time-domain waveform, amplitude and envelope spectra of the most effective component$FIBF1$. From the result shown in Fig. 20c, we can see the characteristic frequency demodulated from the amplitude spectrum of $FIBF1$ centred on the high-frequency resonance band (3.5to4[kHz]) shown in Fig. 20b. Three clear peaks of f_o can be identified from Fig. 20c, and the first is the outer ring fault frequency ($f_o = 108$[Hz]), and the second is two times the outer ring fault frequency ($2f_o = 216$[Hz]), the third peak is ($3f_o = 324$[Hz]). The proportion values of characteristic frequencies f_i and f_o in the spectrum of sig_{OR0} are given by $FCFR_i = 5.35$

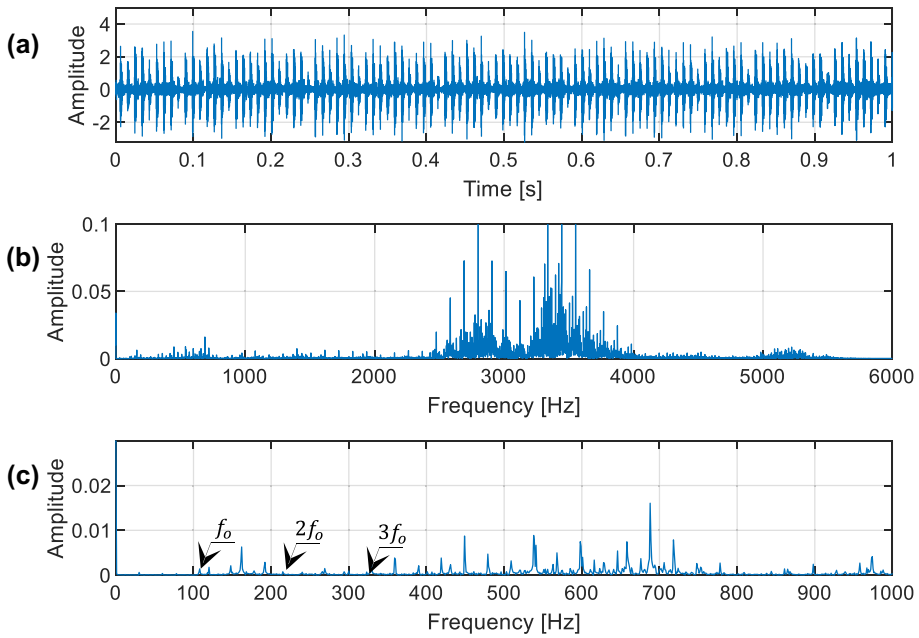


Fig. 18 Measured vibration signal sig_{OR0}: **a** Time-domain waveform; **b** Frequency-domain waveform; **c** Enlarged view of the frequency-domain waveform ($f_o = 107.36$[Hz])

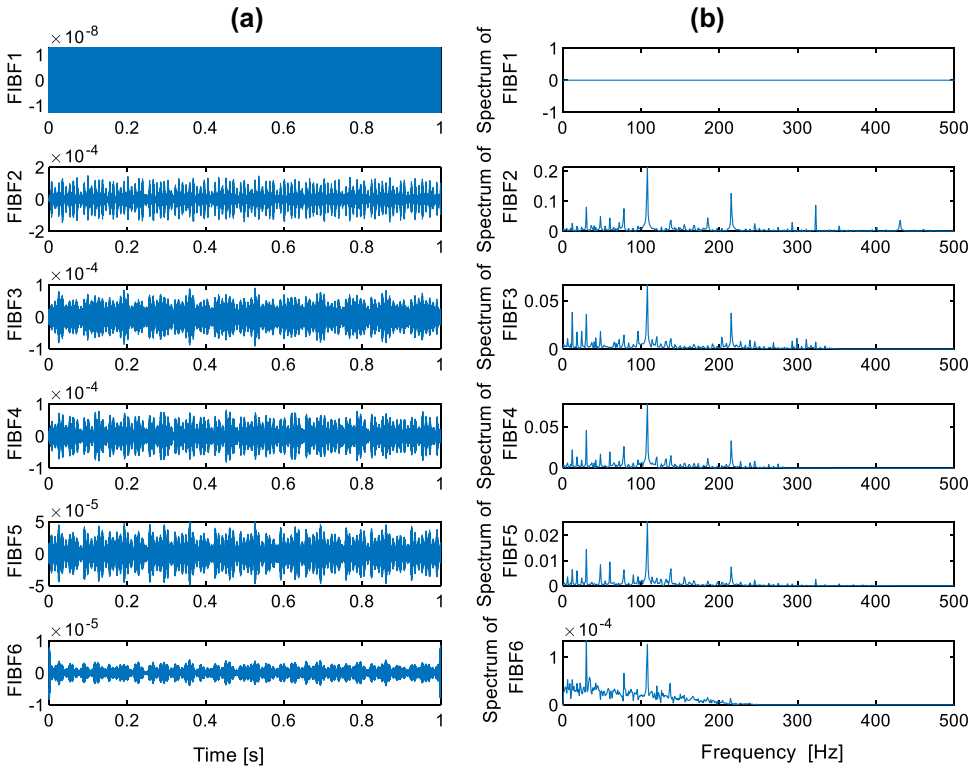


Fig.19 Decomposition results of the measured signal sig_{OR0} using FDM-TEO, **a** Waveform of time-domain of some components $FIBF$; **b** Envelope spectrum of each FIBF

and $FCFR_o = 37.33$, respectively. Overall, the rotational frequency F, the characteristic frequency f_o, and their harmonics are identified on the envelope spectrum. On the other hand, the inner ring fault frequency f_i and its harmonics are undetectable. Therefore, we can easily deduce that the bearing from which this signal originates contains an outer ring fault and that there is no inner ring fault. Consequently, the fault characteristic is extracted by the proposed method.

4.4.4 Bearing Without Fault (Normal)

The spectral envelopes of effective $FIBFs$ extracted from the normal bearing vibration signals (faultless) obtained by $FDM\text{-}TEO$ are shown in Fig. 21. Where, in the four signals sig_{FL0},sig_{FL1},sig_{FL2} and sig_{FL3} no characteristic frequency related to the fault can be observed from the $FIBF$

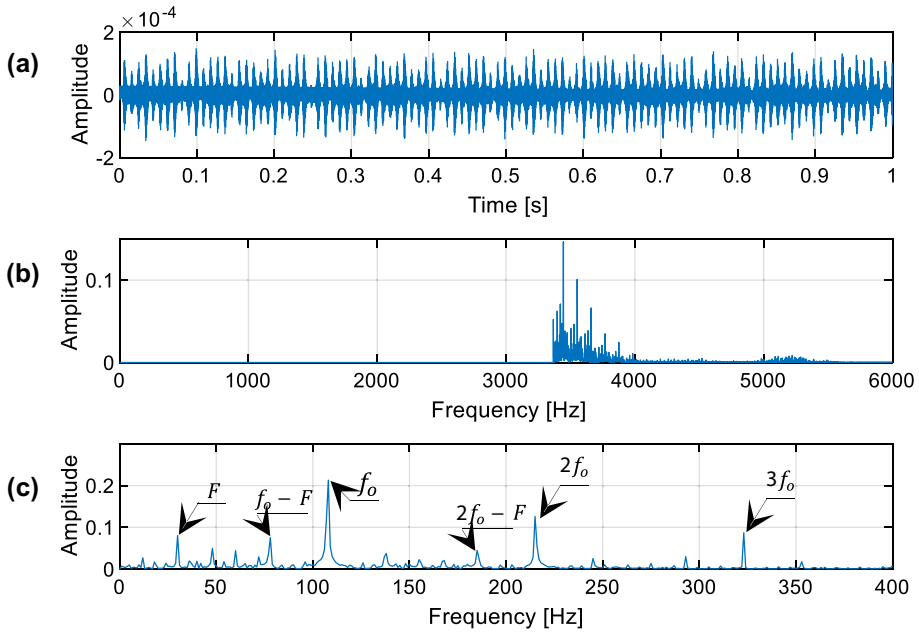


Fig. 20 Spectra of the first component $FIBF1$ obtained by FDM-TEO of signal sig_{OR0}: **a** Time-domain waveform; **b** Frequency-domain waveform; **c** Envelope spectrum ($f_o = 107.36$[Hz] fault frequency, $F = 29.95$[Hz] shaft frequency)

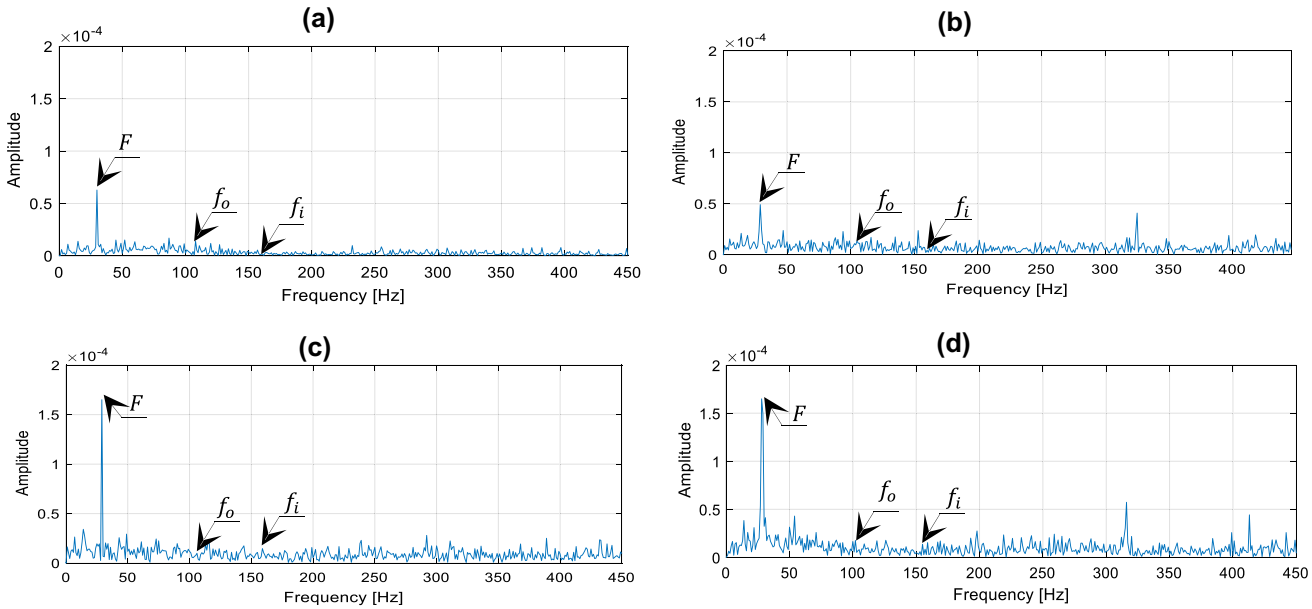


Fig. 21 Spectra of the effective $FIBF$ obtained by FDM-TEO of normal bearing vibration signals: **a** sig_{FL0} (where $f_o = 107.36$[Hz], $f_i = 162.19$[Hz] and $F = 29.95$[Hz]); **b** sig_{FL1} (where $f_o = 105.87$ [Hz], $f_i = 159.93$[Hz] and $F = 29.53$[Hz]); **c** sig_{FL2} (where $f_o = 104.53$[Hz], $f_i = 157.94$[Hz] and $F = 29.17$[Hz]); **d** sig_{FL3} (where $f_o = 103.36$[Hz], $f_i = 157.94$[Hz] and $F = 28.83$[Hz])

Table 6 Largest $FCFR_i$ and $FCFR_o$ of each measured signals obtain by proposed approach

Parameters	Signals											
	sig_{IR0}	sig_{IR1}	sig_{IR2}	sig_{IR3}	sig_{0R0}	sig_{0R1}	sig_{0R2}	sig_{0R3}	sig_{FL0}	sig_{FL1}	sig_{FL2}	sig_{FL3}
$FIBFN°$	65	63	55	18	02	13	07	05	02	02	02	02
$FCFR_i$	24.58	39.01	52.20	26.09	5.35	1.93	3.24	5.43	4.85	4.24	2.97	4.36
$FIBFN°$	67	58	47	21	02	11	04	05	02	02	02	02
$FCFR_o$	7.27	4.18	3.26	4.54	37.33	27.86	35.41	44.29	4.83	4.42	4.19	2.92

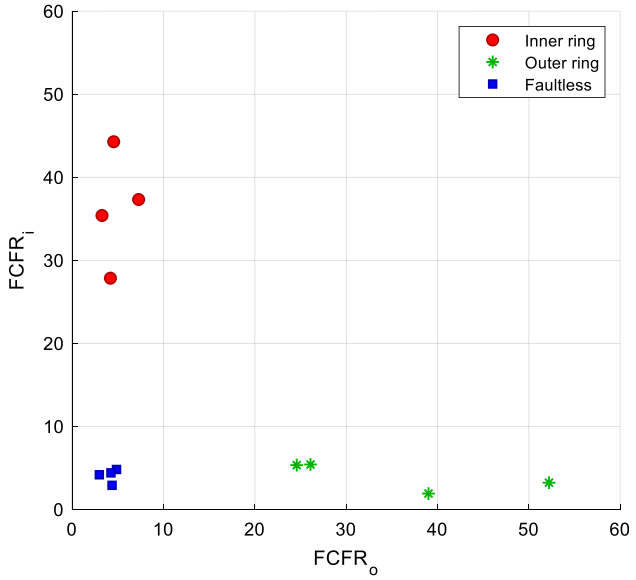


Fig. 22 Diagram of cluster analysis based on FCFR

frequency spectra. So, we can deduce that this bearing is in normal working condition.

4.4.5 Fault Extraction Based on FCFR and FDM-TEO

Table 5 lists the signal characteristics used in this subsection, and Figs. 13 and 14 demonstrate their time and frequency representations. The characteristics of all the signals used in this subsection are specified in Table 5, and their two representations, in the time and the frequency domains are shown in Figs. 13 and 14, respectively. The same steps that we carried out previously on the signals sig_{IR0} and sig_{OR0} are applied to these signals. In other words, all signals are processed by the proposed method. The frequency parameters $FCFR_i$ and $FCFR_o$ of all effective components are used to generate the vector of fault characteristics (Table 6).

Table 6 shows the $FCFR_i$ and $FCFR_o$ of the twelve signals studied in this subsection. For example, the effective $FIBF$ of sig_{IR2} decomposed by $FDM\text{-}TEO$, which contains the largest characteristic frequency $f_i = 157.94$[Hz], is that of the FIBF55, and its values are $\text{FCFR}_\text{i} = 52.20$ and $\text{FCFR}_\text{o} = 3.26$. Figure 22 shows the successful classification of bearing faults because the different signals are located at different places on the characteristic surface. Therefore, the extraction of fault characteristics based on the proposed $FDM\text{-}TEO$ method can detect the bearing fault effectively.

Furthermore, Table 7 presents the average value of the fault frequency rates ($FCFR_i$ and $FCFR_o$). We can see that these values (rates) for normal bearing are low (less than 5). The occurrence of a bearing fault leads to a significant increase in the corresponding fault frequency component. Therefore, the average values of the inner ring fault frequency

Table 7 Average value of the $FCFR_i$ and $FCFR_o$ in diverse bearing situations

Average value of the FCFR	*Types faults*		
	Faultless	*Inner ring*	*Outer ring*
$FCFR_i$	*4.10*	*35.47*	*6.06*
$FCFR_o$	*4.09*	*7.28*	*36,22*

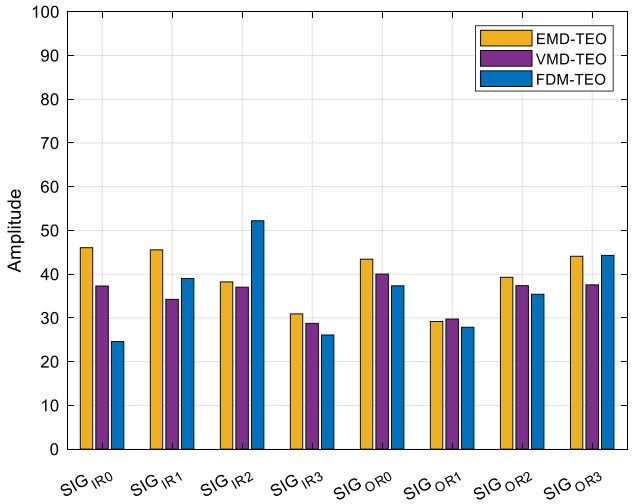


Fig. 23 The FCFR_fi and FCFR_fo of bearing vibration signals with faults in the inner and outer rings, respectively, obtained by the different methods

rates are $FCFR_i = 35.47$ and $FCFR_o = 7.28$. However, the average values of the outer ring fault frequency rates are $FCFR_i = 6.06$ and $FCFR_o = 36, 22$. These results can determine the discrimination threshold δ_d between inner ring fault bearings, outer ring fault bearings and normal bearings. Overall, it is not easy to determine a reliable threshold for fault diagnosis without false alarms or missed alarms, and for the practical importance of the threshold, this requires many samples used for each condition.

4.5 Comparison and Discussion

To show that FDM-TEO is an excellent way to find problems with bearings, we use it on vibration signals from bearings with faults in both the inner and outer rings and, simultaneously, compare it with other methods. (EMD-TEO and VMD-TEO).

The ensemble SIG_{IR0} through SIG_{IR3}, including bearing vibration signals with inner ring faults, is the first ensemble in which these methods are applied. All values of $FCFR_{fi}$ are plotted in Fig. 23 and shown in Table 8's first four rows. As can be seen, FDM-TEO yields an excellent value for "$FCFR_{fi}$" for "SIG_{IR0}" than the values acquired

Table 8 The $FCFR_{fi}$ and $FCFR_{fo}$ of bearing vibration signals with faults in the inner and outer rings, respectively, obtained by the different methods

Parameters	Signals	Methods		
		$EMD-TEO$	$VMD-TEO$	$FDM-TEO$
$FCFR_{fi}$	SIG_{IR0}	46.0476	37.2928	24.5829
	SIG_{IR1}	45.5615	34.25	39.0197
	SIG_{IR2}	38.2333	37.0253	52.207
	SIG_{IR3}	30.9176	28.7519	26.0974
$FCFR_{fo}$	SIG_{OR0}	43.4316	40.0305	37.3358
	SIG_{OR1}	29.1865	29.7359	27.8663
	SIG_{OR2}	39.2928	37.3698	35.4107
	SIG_{OR3}	44.0969	37.5544	4,42,991

by the other two methods. The values acquired by the EMD-TEO are higher than those obtained by the other methods for the other three signals. In general, the $FCFR_{fi}$ s of the three methods are close, with a slight superiority of FDM-TEO over VMD-TEO, and EMD-TEO over both. These results are according to the $FCFR_{fi}$ average values obtained by the three methods, which are 40.19 by EMD-TEO, 34.33 by VMD-TEO and 35.47 by FDM-TEO.

Next, these methods are applied to bearing vibration signals with faults in the outer ring (SIG_{OR0} to SIG_{OR3}). The $FCFR_{fO}$ of all signals are shown in the last four rows of Table 8 and Fig. 23 as a graph. When we look at this set the same way we looked at the last set, we get the same result: the FCFRs of the three approaches are close, with FDM-TEO slightly beating VMD-TEO and EMD-TEO over both. These results compare the three methods' average FCFR values, which are 39.00 for EMD-TEO, 36.17 for VMD-TEO, and 36.23 for FDM-TEO.

5 Conclusion

This paper presents an alternative approach that combines FDM, TEO and FCFR to study bearing vibration signals for fault extraction. Initially, we use FDM to decompose the vibration signal. The next step is to use the TEO to detect the envelopes and the FFT to determine their spectra. The greater FCFR value of each component's envelope determines the most effective component. The "FCFR" values of the effective components are significant features for fault extraction from bearing vibration signal < ls.

The methodology's effectiveness is tested in two distinct ways: applying it to simulated and real vibration signals and comparing it to similar recent methods. It is possible to draw the following inferences from the data shown thus far.

(1) The suggested approach is based on FDM, which differs from EMD and VMD because it is not experimental and does not call for parameter presets.
(2) The suggested approach also uses TEO for envelope extraction, which benefits a narrow time window and a straightforward mathematical expression, as discussed in Sect. 2.3. As a result, the suggested technique is highly effective and has low computational complexity. The suggested approach is ideal for real-time problem diagnostic systems that require online monitoring.
(3) Additionally, the FCFR metric is used to evaluate fault information in the proposed approach, which, in contrast to other indicators, can automatically contain the greatest information about fault frequency (see Sect. 2.4 for more details).

The comparison investigation we conducted for this work showed that despite all the benefits mentioned above of the suggested technique and its slight superiority over VMD, EMD still performed somewhat better. As a result, we will be working to enhance the suggested method's FCFR outcomes so that it can compete with EMD.

Acknowledgements This work is supported by the Directorate General for Scientific Research and Technological Development (DGRSDT) of Algeria. We state our gratitude to the Case Western Reserve University for providing free access to their Database.

References

1. Adams, M. L.: Rotating machinery vibration : from analysis to troubleshooting, Second edition CRC Press Taylor & Francis Group (2009), ISBN 978–1–4398–0717–0
2. Albrecht, P.F., Appiarius, J.C., McCoy, R.M., Owen, E.L., Sharma, D.K.: "Assessment of the reliability of motors in utility applications–updated. In: IEEE Energy Conversion (1986) Available at: http://ieeexplore.ieee.org/stamp/stamp.jsp?tp=&arnumber=4765668.
3. Rubini, R.; Meneghetti, U.: Application of the envelope and wavelet transform analyses for the diagnosis of incipient faults in ball bearings. Mech. Syst. Signal Process. **15**(2), 287–302 (2001). https://doi.org/10.1006/mssp.2000.1330

4. Singh, P.; Joshi, S.D.; Patney, R.K.; Saha, K.: The Fourier decomposition method for nonlinear and non-stationary time series analysis. Proc. R. Soc. (2017). https://doi.org/10.1098/rspa.2016.0871
5. Vamsi, I.; Sabareesh, G.R.; Penumakala, P.K.: Comparison of condition monitoring techniques in assessing fault severity for a wind turbine gearbox under non-stationary loading. Mech. Syst. Signal Process. **124**, 1–20 (2019). https://doi.org/10.1016/j.ymssp.2019.01.038
6. Wang, T.; Han, Q.; Chu, F.; Feng, Z.: Vibration based condition monitoring and fault diagnosis of wind turbine planetary gearbox: a review. Mech. Syst. Signal Process. **126**, 662–685 (2019). https://doi.org/10.1016/j.ymssp.2019.02.051
7. Dou, C.; Lin, J.: Extraction of fault features of machinery based on Fourier decomposition method. IEEE Access (2019). https://doi.org/10.1109/ACCESS.2019.2960548
8. Smith, W.A.; Randall, R.B.: Rolling element bearing diagnostics using the case western reserve university data: a benchmark study. Mech. Syst. Signal Process. (2015). https://doi.org/10.1016/j.ymssp.2015.04.021
9. Boashash, B.: Estimating and interpreting the instantaneous frequency of a signal-part 1: fundamentals. Proc. IEEE **80**(4), 520–538 (1992). https://doi.org/10.1109/5.135376
10. Code of FDM available at (date of the last access is 4 June 2020) : https://www.researchgate.net/publication/274570245_Matlab_Code_Of_The_Fourier_Decomposition_Method_FDM
11. Maragos, P., Quatieri, T. F., Kaiser, J. F.: Speech nonlinearities, modulations, and energy operators, [Proceedings] ICASSP 91: 1991. In: International Conference on Acoustics, Speech, and Signal Processing (1991) doi:https://doi.org/10.1109/icassp.1991.150366
12. Kvedalen, E.: Signal processing using the Teager Energy Operator and other nonlinear operators. In: Thesis, University of Oslo Department of Informatics (2003). Online at http://folk.uio.no/eivindkv/ek-thesis-2003-05-12-final-2.pdf
13. Kaiser, J. F.: On a simple algorithm to calculate the "energy" of a signal. In: International Conference on Acoustics, Speech, and Signal Processing (1990) doi:https://doi.org/10.1109/icassp.1990.115702.
14. Deng, M.; Deng, A.; Zhu, J.; Zhai, Y.; Sun, W.; Chen, Q.; Liu, Y.: Bandwidth fourier decomposition and its application in incipient fault identification of rolling bearings. Meas. Sci. Technol. (2019). https://doi.org/10.1088/1361-6501/ab4069
15. Zhang, L.; Xiong, G.; Huang, W.; Zhang, L.; Xiong, G.; Huang, W.: New procedure and index for the parameter optimization of complex wavelet based resonance demodulation. J. Mech. Eng. **51**, 129–138 (2015). https://doi.org/10.3901/JME.2015.03.129
16. Rilling, G.; Flandrin, P.; Gonçalvès, P.: On empirical mode decomposition and its algorithms. Proc. IEEE-EURASIP Workshop Non Linear Signal Image Process NSIP **3**, 8–11 (2003)
17. Rilling, G.; Flandrin, P.: One or two frequencies? The empirical mode decomposition answers, signal processing. IEEE Trans. **56**(1), 85–95 (2008)
18. Wan, S.; Zhang, X.: Teager energy entropy ratio of wavelet packet transform and its application in bearing fault diagnosis. Entropy **20**(5), 388 (2018). https://doi.org/10.3390/e20050388
19. Wang, D.T.; Peter, W.T.; Yiu, L.: A morphogram with the optimal selection of parameters used in morphological analysis for enhancing the ability in bearing fault diagnosis. Meas. Sci. Technol. (2012). https://doi.org/10.1088/0957-0233/23/6/065001
20. Case Western Reserve University Bearing Data Center Website (date of the last access is 4 June 2020) : https://csegroups.case.edu/bearingdatacenter/pages/download-data-file
21. Hemati, A.: A case study: fluting failure analysis by using vibrations analysis. J. Fail. Anal. Prev. **19**, 917–921 (2019). https://doi.org/10.1007/s11668-019-00715-w
22. Randall, R.B.; Antoni, J.: Rolling element bearing diagnostics a tutorial. Mech. Syst. Signal Process. **25**(2), 485–520 (2011). https://doi.org/10.1016/j.ymssp.2010.07.017
23. Boudiaf, A.; Moussaoui, A.; Dahane, A., et al.: A comparative study of various methods of bearing faults diagnosis using the case western reserve university data. J. Fail. Anal. Prev. **16**, 271–284 (2016). https://doi.org/10.1007/s11668-016-0080-7

Springer Nature or its licensor (e.g. a society or other partner) holds exclusive rights to this article under a publishing agreement with the author(s) or other rightsholder(s); author self-archiving of the accepted manuscript version of this article is solely governed by the terms of such publishing agreement and applicable law.